Natural Hazards
and Earth System
Sciences
Discussions

# Implications from palaeoseismological investigations at the Markgrafneusiedl Fault (Vienna Basin, Austria) for seismic hazard assessment

Esther Hintersberger[1], Kurt Decker[1], Johanna Lomax[2,3], Christopher Lüthgens[2]

[1]Department of Geodynamics and Sedimentology, University of Vienna, 1090 Vienna, Austria
[2]Institute of Applied Geology, University of Natural Resources and Life Sciences (BOKU), 1190 Vienna, Austria
[3]Department of Geography, Justus Liebig University Gießen, 35390 Giessen, Germany

*Correspondence to*: Esther Hintersberger (esther.hintersberger@univie.ac.at)

**Abstract.** Including faults into seismic hazard assessment depends strongly on their level of seismic activity. Intraplate regions are characterized by low seismicity, so that the evaluation of existing earthquake catalogues does not necessarily reveal all active faults that contribute to seismic hazard. In the Vienna Basin (Austria), moderate historical seismicity (Imax/Mmax = 8/5.2) concentrates along the left-lateral strike-slip Vienna Basin Transfer Fault (VBTF). In contrast, several normal faults branching out of the VBTF show neither historical nor instrumental earthquake records, although geomorphological data indicate Quaternary displacement along those faults. Here, we present a palaeoseismological dataset of three trenches crossing one of these splay faults, the Markgrafneusiedl Fault (MF), in order to evaluate the seismic potential of the fault. Comparing the observations of the different trenches, we found evidence for 5-6 major surface-breaking earthquakes during the last 120 ka, with the youngest event occurring at around ~14 ka before present. The inferred surface displacements lead to magnitude estimates ranging between M=6.2±0.3 and M=6.8±0.1. Data can be interpreted by two possible event lines, with event line 1 showing more regular recurrence intervals of about 20-25 ka between the earthquakes with M≥6.5, and event line 2 indicating that such earthquakes cluster in two time intervals in the last 120 ka. Event line 2 appears more plausible. Trench observations also show that structural and sedimentological records of strong earthquakes with small surface offset have only low conservation potential. Vertical slip rates of 0.03-0.04 mm/a derived from the trenches compare well to geomorphically derived slip rates of 0.015-0.085 mm/a. Magnitude estimates from fault dimensions suggest that the largest earthquakes observed in the trenches activated the entire fault surface of the MF including the basal detachment that links the normal fault with the VBTF. The most important implications of these paleoseismological results for seismic hazard assessment are that: (1) The MF needs to be considered as a seismic source irrespective of the fact that it did not release historical earthquakes. (2) The maximum credible earthquakes in the Vienna Basin should be considered to be about M=7.0. The MF is kinematically and geologically equivalent to a number of other splay faults of the VBTF. It must be assumed that these faults are potential sources of large earthquakes as well. The frequency of strong earthquakes near Vienna is therefore expected to be significantly higher than the earthquake frequency reconstructed for the MF.
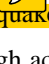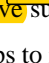
## 1 Introduction

During the last years, earthquakes tend to "surprise" seismologists, either by unexpectedly high magnitudes (e.g., Sumatra Earthquakes 2004, Tohuko Earthquake 2011) or/and by the fact that the generating faults were either unmapped (Christchurch Earthquake 2010) or assumed to be inactive (e.g., Haiti Earthquake 2009). Thus, it seems to be clear that historical and

5   instrumental seismicity data are not sufficient to fully characterize the seismogenic potential of a certain region (e.g., Camelbeeck et al., 2007, Liu et al., 2011). Especially in regions of low to moderate seismicity, mostly in intraplate settings, observations of historical and instrumental seismicity are not sufficient to accurately estimate the rate of earthquake activity (Liu et al., 2011). Therefore, during the last decade, geomorphological and palaeoseismological approaches have been increasingly used to map active faults and to determine the related slip rates (e.g., Clark et al., 2012 in Australia, and Vanneste

10  et al., 2013, for the Lower Rhine graben system in Central Europe). The results of those studies have dramatically changed the picture and the level of seismogenic potential in the analysed regions, mainly in the following aspects: Firstly, palaeoseismological results show that the magnitude for the maximum credible earthquake may be significantly higher than the magnitude for the largest earthquake observed during historical times (e.g, Central Europe north of the Alps, Figure 1B and references mentioned there). Secondly, the amount of active faults that are considered to be capable of generating

15  earthquakes has been increased (e.g., Clark et al., 2012 in Australia). The identification of such "silent" faults as potential seismic sources has become a vital aspect of geological contribution to seismic hazard assessment. Finally, extension of the observed earthquake records raised the question whether faults (especially single faults within fault systems) show regular earthquake patterns during time (characteristic earthquakes occuring in more or less regular time intervals) or if earthquakes occur in so-called super-cycles, where periods of high activity change with intervals of seismic quiescence (Wallace, 1987,

20  Friedrich et al., 2003). Here, we present results of a paloseismological study, where a dormant active fault has been identified close to the city of Vienna (Austria). Even though there is no historical nor instrumental seismicity that has been recorded along this fault, three trenches across the fault show evidence for five surface-breaking earthquakes. Correlation between the trenches and integration of geomorphological and borehole data helps to identify whether the fault tends to more characteristic or super-cycle behaviour.

## 2 Geological setting

### 2.1 The Vienna Basin

The Vienna Basin has formed as a pull-apart basin between the Eastern Alps and the Western Carpathians in the Middle and Upper Miocene (e.g. Royden, 1985; Decker et al., 2005). It is located between two left-stepping segments of the NE-SW

5    striking sinistral strike-slip Vienna Basin Transfer Fault (VBTF, Figure 1). Faulting along this fault system is related to the NE-directed movement of the block east of the Vienna Basin, caused by lateral extrusion of the central Eastern Alps towards the Pannonian Basin (Ratschbacher et al, 1991, Linzer et al, 1997, 2002). GPS data (Grenerczy et al., 2005) and geological reconstruction of Quaternary sediment deposition within the basin (Decker et al., 2005) indicate that the VBTF moves at horizontal velocities between 1.6 and 2.4 mm/y. However, seismic slip rates calculated from cumulative scalar seismic

10   moments for different segments along the fault are quite heterogeneous, varying from 0.5-1.1 mm/a at the southern and northern tips to an apparently seismically totally locked segment in the central part of the basin, the so-called Lassee segment, close to the city of Vienna (Hinsch et al, 2005, Hinsch and Decker, 2011). Fault mapping using 2D/3D reflection seismic, gravity, and geomorphology shows that these seismotectonically defined segments are delimited by major fault bends including a restraining bend (Dobra Voda) and three releasing bends with negative flower structures overlain by Pleistocene pull-apart

15   basins with up to 150 m growth strata (Beidinger and Decker, 2011). The releasing bends are connected by non-transtensive segments. In addition to the overall geometry of the strike-slip fault with releasing and restraining bends, the transfer of displacement to several normal faults splaying from the strike-slip system in the central part of the basin appears to be an important factor controlling fault segmentation. The splay faults formed during the Middle to Upper Miocene formation of the Vienna pull-apart basin (Decker et al., 2005) and seem to be kinematically linked to the VBTF via a common detachment (i.e.,

20   the Alpine floor thrust, Figure 2, Hölzel et al., 2010, Hinsch and Decker, 2011, Beidinger and Decker, 2011). Those secondary splay normal faults seem to have been seismically inactive during historic times. However, geomorphologic and subsurface geophysical data reveal that those faults indeed show Quaternary displacement of several tens of meters (Chwatal et al., 2005; Decker et al., 2005, Weissl et al., 2017). Moderate historical and instrumental seismicity (Mmax ~ 5.3/ Imax = 8) is concentrated along the VBTF with the 1972 Seebenstein (M~5.3), 1906 Dobra Woda (M~5.7) and the ~ AD 350 Carnuntum

25   (M~6) earthquakes being the largest known events (Gutdeutsch et al., 1987; Decker et al., 2006; Lenhardt et al., 2007). The scarcity of strong earthquakes and the generally low to moderate seismicity result in estimations of Mmax for earthquakes in the Vienna Basin might not exceed M = 6.0 to 6.5 (Lenhardt et al., 1995; Procházková and Šimunek, 1998; Sefara et al., 1998; Tóth et al., 2006). However, those estimations are solely based on historical and instrumental seismicity.

Natural Hazards
and Earth System
Sciences
Discussions

Open Access

EGU

## 2.2 The Markgrafneusiedl Fault (MF)

Our palaeoseismological study is focused on the SE-dipping Markgrafneusiedl Fault (MF) in the central part of the Vienna Basin. It is one of six splay normal faults that ~~were generated~~ during the Middle to Upper Miocene formation of the Vienna

5   Basin to accommodate transtension at a releasing bend of this sinistral strike-slip fault (Beidinger and Decker, 2011). The location of the fault, fault displacement and fault dimensions are evident from 2D and 3D industrial seismic (Hinsch et al., 2005, Spahic et al., 2013). An exemplary seismic section is shown in Figure 3. Detailed observations based on 3D industrial seismic data on the fault plane suggests that movement along the MF started on different fault segments that eventually merged together as one larger fault (Spahic et al., 2013). Quaternary fault reactivation is inferred from geomorphological evidence of

10  a linear scarp paralleling the outcrop trace of the fault, high-resolution geophysical profiling (georadar, reflection seismic, geoelectrics; Chwatal et al., 2005) and the ca. 40 m offset of the base of the Quaternary sediments across the MF (Decker et al., 2005). The visible fault scarp falls together with the SE edge of the Gaenserndorf terrace, building a linear geomorphological step of ca. 12 m height in the present-day topography (Figure 3).

Despite this well documented Quaternary displacement along the MF, no historical seismicity is recorded that can be associated

15  with this fault, except for small earthquakes with magnitudes less than 1.0 that have been recorded close to the MF in the last decade. Whether this apparently slowly moving fault can produce larger earthquakes or it is aseismically creeping, is the key question of our study, during which three trenches (from north to south WAG, SDF1, and SDF3) were excavated across the MF between the villages of Markgrafneusiedl and Gaenserndorf, about 15 km from the city limits of Vienna, the Austrian capital. ~~The results show that these normal faults are indeed capable of generating earthquakes and therefore must be~~

20  ~~considered as potential seismogenic sources. In addition, the observations indicate that earthquakes within the Vienna Basin could exceed the maximum magnitudes estimated from historical and instrumental seismicity.~~

## 3 Trenching results

~~In total, we~~ excavated two trenches along the geomorphic fault scarp between the villages of Markgrafneusiedl and Gaenserndorf (Figure 3A). ~~For the exact position of the trenches,~~ 40 MHz ground penetration radar (GPR) profiles were carried

25  out showing the location of the MF at the base of the present-day scarp. In addition, a construction pit of a gas pipeline exposed the northern tip of MF, providing additional, but limited, information. In general, all outcrops show similar characteristics: at all trenching locations, the MF is exposed as narrow (1 - 2 m) fault zone consisting of one or two fault branches striking parallel to the regional strike of the fault scarp of the MF (dip direction/dip: ~120/75). The footwall cut by the MF comprises deposits typical for the Gaenserndorf terrace (Weissl et al., 2017 and references therein). The hanging wall of the trenches expose

30  sequences of almost horizontally layered, fine-graded sediments.

## 3.1 Trenching at SDF1

The 40-m-long, 3-m-wide and up to 4 m deep trench SDF1 was located close to the farm house "Siehdichfür", about 20 km from the city limits of Vienna. It was excavated in a small dry valley at the central part of the NE-SW trending geomorphological fault scarp with the exact location of the MF at its base. Trench mapping ~~in the~~ scale of 1:10 covers both,

5  the entire SW wall of the trench and the section around the fault zone at the NE wall. The trench SDF1 exposed about 30 m of Gaenserndorf terrace deposits in the footwall and ca. 10 m of the hanging wall, divided by the 1.5 m wide fault zone of the SE-dipping MF. The fault zone includes two parallel steeply dipping faults F1 and F2, with F2 reaching almost the present-day surface (see Figure 4).

At the NW part in the footwall, alluvial deposits of the Gaenserndorf terrace are exposed, consisting of coarse gravels and

10  boulders. Pebbles show consistent NW-dipping imbrication throughout the entire footwall section. The inferred dominantly SE-directed paleocurrents are comparable to the flow direction of the Recent Danube. In addition, two approximately 8 m wide sandy ancient river channel fills are observed close to the top of the succession. Another sand lense, only partly exposed at the base of the outcrop, is cut by the fault zone. The uppermost 0.5 m of the terrace deposits directly below the recent soil horizon do not show ~~any~~ horizontal consistency and ~~are most~~ probably reworked and repositioned.

15  In the hanging wall SE of the fault zone, three types of sediments are exposed:

(A) Sequences of horizontal layers of light-grey and light-brown silt and fine sand with varying thicknesses up to 20 cm. Sediments show lamination on cm-scale and intercalations of cm-thick horizons of coarse sand. The layers also include singular well-rounded pebbles and granules aligned in horizontal layers. Some sand/silt layers show fining-upward trends. Carbonate cementation is observed along the top of the uppermost silt layer and along recent root paths. The sediments are intercalated

20  with and onlap on the wedge-shaped colluvial deposits described below. We relate the deposits to high-stage floods in the floodplain of the Pleistocene Danube.

(B) Colluvial wedge deposits and associated tension crack fills. These colluvial sediments are attached to both faults and decrease in thickness towards the SE (i.e., away from the fault scarp; Figure 4). The steep contact with the SE-dipping faults and the thinning of the deposits towards SE results in a wedge-shape of the sediment layers. The tails of wedges 2, 3 and 5 can

25  be followed throughout the exposed part of the hanging wall. All wedges are associated with tension cracks adjacent to the fault, which are filled with the same material as the overlying wedge. Wedge 5 consists of matrix-supported reddish brown medium gravel with a matrix composed mainly by sand and silt together with a low content of clay. Wedge 4 is delimited by a steep irregular boundary adjacent high-stage flood sediments. While wedge 4 comprises brown to reddish brown fine to medium sand with some fine granules and pebbles in a matrix-supported fabric, the latter include rounded pebble-size clasts

30  of the reddish wedge material interpreted as mud balls. We interpret this peculiar contact to result from the partial erosion of the wedge and the wedge tail during high-stage floods and the re-deposition of the colluvial material by fluvial processes or small slumps. Wedge 3 consists well-sorted reddish brown middle sand with a few pebbles (fine gravel) showing lamination dipping away from Fault 1. These three wedges contrast by their red and reddish-brown colour from the intercalated high-

stage flood deposits. The sedimentary material was identified as redeposited soil, which by its colour, resembles ferretto soils (5YR 4/4, Y5YR 5/4 and 5YR 58 of the standard soil colour chart; L. Smolíková, pers. comm.), which derived from the soil cover of the terrace gravels in the footwall of the MF. While the lower three colluvial wedges (3-5) are bounded by F1, wedge 2 is attached to F2 and overlies the trace of F1as well as the deposits of wedge 3. The wedge consists of large well-rounded

5  pebbles and cobbles oriented sub-horizontally in a grain-supported fabric, similar to the terrace deposits found in the foot wall. (C) Fine-grained alluvium and loess. The uppermost part of the sedimentary succession of both the hanging wall and the footwall consists of several thin layers of sand and fine gravel overlain by up to 1 m of unstructured silt and fine sand. The latter is transitional to the overlying dark brown to black soil horizon. The succession is interpreted as alluvium of the dry valley and loess-like sediments or redeposited loess. Fault 2 offsets the alluvial sand layers for about 15 to 20 cm, but terminates

10  within the overlying loess-like sediments several cm above the base of the layer.

Structural data obtained from the two faults exposed in the outcrop show that both faults strike parallel to the regional strike of the fault scarp of the MF. The faults are marked by bands of pebbles with preferred orientations parallel to the fault planes. Pebbles in the 75 cm thick fault block between the two faults show orientations, which geometrically resemble S-C-type fabrics. Deformation bands are found in the sand wedges 3 and 4 and the related tension cracks. Detailed mapping reveals that

15  these microfaults do not penetrate into the colluvial wedge 5 most probably due to the higher clay content of these sediments. The deformation bands show orientations consistent with the main faults of the outcrop. At the lower parts, the deformation bands are dipping parallel to F1 (dip direction/dip 130/80). The upper parts of the deformation bands are rotated away from the fault resembling horsetail splays. The orientations of the sub-vertical deformation bands vary between 303/78 and 330/78. In addition to some major deformation bands, which are traced for about 1 m across the profile, there are shallow dipping

20  deformation bands with comparably large normal offsets up to several mm (145/20). Finally, small-scale normal faults with displacement in the order of several centimeters are observed within the uppermost layers that have been also affected by the youngest displacement along F2 (Figure 5E).

### 3.1.1 Evidences for seismic events observed within trench SDF1

Offset of alluvial sand layers at the tip of F2 provides direct evidence for the youngest surface-breaking slip event A1. The

25  small-scale faults observed at the same stratigraphic level are further indications for an earthquake at this fault. A1 is offsets and postdates colluvial wedge 2. The observed colluvial wedges, their geometrical relation to the adjacent faults, and the sediment-filled extension fissures prove four distinct events (A2 to A5) of rapid co-seismic displacement at the MF. In addition, the existence of deformation bands within the sandy colluvial wedges 3 and 4 indicates further deformation of both wedges during younger slip events at the MF. Among the earthquakes excavated by the trench, only slip associated with A1 is directly

30  constrained by the offset of layers correlated across Fault 2. Evidence for the earthquakes A2 to A5 comes from the colluvial wedges 2 to 5 and the refilled tension cracks 2' to 5' below the wedges. Following the generally accepted rule of thumbs that colluvial wedge height is approximately half of the surface displacement of an earthquake (McCalpin, 2008), the measured maximum thickness of each colluvial wedge can be used to estimate the minimum displacement for the associated event.

## 3.2 Trenching at SDF3

Trenching in the Vienna Basin continued with the opening of a second trench SDF3 across the same fault. This 33 m long, 3 m wide and up to 5 m deep trench is located about 1.5 km SW of the first trench SDF1. Trench mapping in the scale of 1:10 covers both, the entire W wall of the trench and the section around the fault zone exposed in the terraced E wall (Figure 6).

5    The about 0.5 m wide fault zone of the SE-dipping MF divides the N-S trending trench into two parts. The footwall W of the fault mainly consists of gravels of the Gaenserndorf terrace whereas the hanging wall in the E shows a succession of fluvial sediments, colluvial deposits originating from the uplifted footwall and reworked loess-like sediments.

The footwall mainly consists of poorly sorted, well rounded sandy gravels within a grain-supported fabric. Components mostly include metamorphic rocks, gneisses, quartzite along with minor sandstone and limestone. The few magmatic components

10    found within the gravels completely weathered. The lower 1-1.5 m of the terrace excavated in the trench contains coarse cobbles with diameters up to 25 cm. The upper part shows typical characteristics of braded river deposits, including crossbedding of better-sorted gravel layers intercalated with sand layers of up to 0.5 m of thickness and several meters of lateral extent. Furthermore, the part consists of gravel and small cobbles with diameters up to 10 cm. All layers show a slight inclination towards the SE. Throughout the terraces deposits, vadose gravitational carbonate cementation, so-called dripstone

15    cementation, along the lower side of larger gravels is observed.

The hanging wall consists of horizontally layered sediments of different origin. In the following, we describe the most important units of the hanging wall, starting with the lowermost unit. Unit 1 consists of intercalated beige to grey, medium to fine sand and gravel layers consisting of well-rounded, poorly sorted clasts. The thickness of the layers varies between ~3 cm and 20 cm, whereas the sand layers are generally thicker than the intercalated gravel layers. This sequence is the result of

20    alternate high-stage Danube floods (sand layers) and erosional events transporting gravels from the footwall into the hanging wall. Those erosional impulses may be triggered by heavy-rainfall events. The contact to the overlying unit 2 is clearly identified. Unit 2 consists of matrix-supported conglomerate with clay-rich, Fe-rich red fine sandy matrix and poorly sorted, well-rounded clasts with diameters up to 15 cm. Grain sizes decrease with increasing distance from the fault, as well as the layer thickness from 70 cm directly at the fault to less than 50 cm further away. The contact to the overlying unit 3 is diffuse.

25    Unit 3 consists of red clay-rich Fe-rich fine sand with intercalated layers and up to 5 cm thick lenses of brownish slightly coarser sand without clay or Fe components. The layering shows a slight inclination of a few degree towards the NW, i.e., towards the fault. The material is typical for distal flood basin deposits of fluvial environments. A few well rounded clasts with diameters of 2 - 20 cm have been observed. Their distribution suggests that they may be dropstones. The contact between this unit and the overlying unit 4 is characterized by a generally horizontal sharp contact, which has been affected by

30    liquification, either caused by the occurrence of an earthquake or by the deposition of the overlying coarse gravels over the still water-bearing sediments of unit 4. Furthermore, a burrow of small animals, refilled with beige coarse sand is observed at the bottom of this layer. Unit 4 consists of grain-supported conglomerate with well-rounded, poorly sorted cobbles with grain sizes up to 10 Those gravels originate from the footwall and form a colluvial wedge, which decreases in thickness with

increasing distance to the fault. Unit 5 consists olive-coloured medium sand with rare mica components. This 10 cm thick unit decreases in thickness towards the fault. This fact, together with the colour of the sand, suggests that it is a flood deposits of the Danube. Unit 6 covers both, the hanging and the foot wall and consists of a matrix-supported conglomerate with silt matrix and around 25% of components that consist of poorly sorted, well-rounded pebbles with grain sizes up to 3 cm. The silt matrix

5    consists of reworked loess that has probably eroded from the footwall, including smaller clasts from the Gaenserndorf terrace. In the top of this unit, secondary carbonate cemented a horizontal layer of up to 30 cm thickness. The layer is observed throughout the entire hanging wall. Carbonate cementation occurs due to meteoric waters dissipating carbonate from the upper layers and precipitating it at lower pH values in greater depth. Conjugated planar carbonate fissures of up to 60 cm length branch off from the cemented layer. They strike approximately parallel to the orientation of the MF. Unit 7 is the AC soil

10   horizon, consisting of a matrix-supported conglomerate of fine sand and 30-40% of components containing partly angular and rounded pebbles with grain sizes up to 2 cm.  The contact to both the underlying and overlying units, is rather diffuse. Finally, unit 8 is the A soil horizon that increases in thickness with increasing distance to the MF. Its thickness coincides with a layer of silt or loess that has been reworked as soil.

Structural data obtained from the outcrop show that both faults strike parallel to the regional strike of the fault scarp of the MF

15   (dip direction/dip: 116/74). The MF is marked by the contact between the footwall gravels and the more sandy deposits of the hanging wall. In addition, at the lower 1.5 m, clasts within a zone of about 50 cm to the fault are rotated parallel to the fault (dip direction/dip: 116/69). The upper part of the MF is only marked by a small band of rotated clasts. However, in this upper part of the fault, layers that can be correlated on both sides of the fault, are displaced by about 15 cm and, therefore, indicate the youngest movement along the fault. In addition to the main faults, several conjugated sets of normal faults are observed

20   within lower units of the hanging wall. These faults are consistently oriented parallel to the MF. The NW-dipping antithetic faults (dip direction / dip: 303/79) are generally longer than the SE-dipping faults (dip direction / dip: 137/72). Displacement observed along the faults is in the range of about 10 cm in the lowest unit 1, and up to 1 cm in the reddish clay-rich unit 3. None of the small faults seem to penetrate into the gravels overlying the reddish clay-rich sand layer (unit 3). Within this layer, the small faults are recognised as a few mm thin deformation bands, most probably filled with carbonate cement, and show

25   almost no displacement. . The sand layers of the lowermost unit 1, consisting of intercalated layers of sand and matrix-supported gravels, comprises small deformation bands with lengths up to 20 cm. They are arranged parallel to the small faults and accordingly dip towards the SE or the NW.

### 3.2.1 Evidences for seismic events observed within trench SDF3

The MF within the trench SDF3 is a very narrow fault zone of 0.5 m width at its lowest point excavated within the trench, and

30   reduces to a fault represented only by a few rotated clasts in the uppermost part. However, this reduction of thickness is not a continuous, but occurs in distinct steps. Those steps can be related to different earthquakes; The oldest earthquake that can be identified within the trench is B5 that created a colluvial wedge along the fault trace F3. This fault trace is then covered by another colluvial wege, which was most probably created by movement along F2 during B4. Evidence for the event B3 is a

tension crack between F2 and F2', that is also identified by the thin sand layer that is smeared into the crack, parallel to F2'. B2 is identified by a ~ 0.8 m thick colluvial wedge. However, the fault strand bounding this colluvial wedge is not obvious. This situation may be explained by the following scenario: In the case that coseismic surface rupture offset unconsolidated water-saturated sandy gravel, it seems plausible that no long-standing free surface and colluvial wedge adjacent to the fault

5    plane could form. Instead, the offset soft sediment may have collapsed during or shortly after the earthquake forming a wedge-shaped deposit, which overlies the uppermost part of the ruptured fault. The same geometry may result from geli-solifluction under periglacial conditions when material glides down to the hangingwall destroying a previously formed free surface. The latter scenario is supported by the observation of a smooth change between the horizontal layers of the terrace and the inclined layers in the colluvial wedge. The described situation allows for two different interpretations of the surface displacement of

10   B2. Interpreting the wedge-shaped deposit as a classical colluvial wedge adjacent to a fault plane which is not readily seen due to unfavourable outcrop conditions, a minimum displacement can be estimated by multiplying the maximum wedge height by two (McCalpin, 2008), which would result in a displacement of 2 x 0.8 m = 1.6 m for B2. In case that the wedge formed by free surface collapse of water-saturated sediment or gelifluction the coseismic surface displacement be approximately the same as the colluvial wedge height, i.e. 0.80 m.

15   Insights for the youngest event B1 in the trench are more obvious. Displacement of the upper layers for ~ 10 cm affected all layers excluding only the soil horizons (units 7 and 8), suggesting that even with such a small displacement of only 10 cm, the event B1 ruptured the surface.

### 3.3 Trenching at WAG

Additional evidence for active faulting at the MF are available from the construction pit of a gas pipeline, which crosses the

20   northern part of the fault scarp close to the city of Gaenserndorf, 6 km north of trench SDF. The outcrop revealed a 1-m-wide localized fault zone (Figure 8). The fault cuts light-grey gravel and sand of the Gaenserndorf Terrace and overlying loess-like sediments (silt, fine to medium grained sand) constituting its footwall. The exposed hanging wall succession includes poorly sorted sandy gravel, which is then overlaid by a banded sequence of silty sediments. This cover layer can be found all along the pipeline construction pit and has been described in detail by Weissl et al. (2017). Both the hanging wall and footwall are

25   overlain by c. 30-50 cm thick brown soil, which has been removed prior to the excavation. The exposed fault zone consists of several deformation bands within the terrace gravel marked by aligned and fractured pebbles, faults offsetting sand layers, and faults offsetting the contact between gravel units and the overlying cover silts (Figure 9). Several sheared pebbles indicate dip-slip movement along the deformation bands. The displacements of these faults are between 10 and 20 cm. On the southern wall a fault cuts up through the entire silty section to the base of the overlying soil, offsetting a thin white layer within the

30   upper part of the cover silty sediments by about 20 cm.

## 4 Luminescence dating

Luminescence dating is commonly used to date the time that feldspar and/or quartz grains in sandy or silty sediments were not exposed to sunlight, and therefore to constrain deposition ages of those sandy or silty sediment bodies. Regarding the physical background and the basics of luminescence dating methods we refer to previously published review papers of Preusser et al.

5    (2008), Wintle (2008), and Rhodes (2011).

### 4.1 Sampling and experimental setup

In analogy to the procedure described by Weissl et al. (2017), samples were collected in the field by driving an opaque steel cylinder into the freshly cleaned sediment surface and transferring the material into light tight plastic bags. All subsequent sample preparation steps were conducted under subdued red light conditions in the Vienna laboratory for luminescence dating.

10    Samples were first dried and dry sieved. The grain size fraction of 100 - 200 mm was used for further preparation steps. The material was subjected to 15% HCl to remove carbonates, treated with $Na_2C_2O_4$, (0.01 N) to disperse clay particles, and with 10% $H_2O_2$ to dissolve organic components. Quartz and feldspar separates were obtained by density separation using LST Fastfloat.

In this study, we used potassium-rich feldspar as luminescence dosimeters for age determination. All fractions were measured

15    with small aliquots of 1 mm diameter mask size using a grain size fraction of 100 - 200 mm. All measurements for determination of the equivalent dose were conducted in the Vienna laboratory for luminescence dating on RISØ TL-OSL DA 20 automated luminescence reader systems (Bøtter-Jensen et al., 2000, 2003). For De determination of the feldspar fraction, a conventional SAR IRSL protocol was applied (Wallinga et al., 2000; Blair et al., 2005), using a preheat of 250°C for 20 s and a stimulation at 50°C for 300 s. Stimulation was carried out with IR-LEDs, and signals were detected after passing through a

20    blue interference filter (410 ± 20 nm). Doses were determined on small multi-grain aliquots (mask-size 1mm). Over-dispersion (Galbraith et al. 1999) was below 11% in all samples confirming a generally well-bleached nature of the sediments. It needs to be stressed that the feldspar based ages were not corrected for fading. Fading describes an anomalous signal loss very commonly observed for potassium-rich feldspar (Wintle, 1973). If not corrected for, fading leads to the underestimation of the burial age. However, samples from the same study area investigated by Weissl et al. (2017) showed little or no fading, as

25    demonstrated by a comparison between quartz and feldspar luminescence ages. Nevertheless, all ages presented here need to be treated with caution for potential age underestimation. Radionuclide concentrations for dose-rate estimation were determined on ~900 g of bulk sediment using high resolution, low-level gamma-spectrometry. Samples were first dried, homogenised and stored in sealed Marinelli beakers (500 ml, about 1 kg dry weight) for at least a month to establish secondary secular radon equilibrium. Measurements were conducted using a Canberra HPGe detector (40% n-type). Relevant

30    luminescence data is listed in Table 2.

## 4.2 Sedimentary and tectonic context

In general, luminescence dating results fit well to the stratigraphic hanging wall sedimentary sequences observed in both trenches, showing continuous decrease in age from the bottom towards the top. In addition, ages derived for the Gaenserndorf terrace in the footwall fit well with other ages from this terrace (Weissl et al., 2017).

Regarding to trench SDF1, Event A1 is well constraint between 13.8 ± 1.4 ka and 16.3 ± 1.8 ka by samples from an offset sand layer and overlying undeformed sediments. Events A2 and A3 are bracketed by the ages inferred for A1 and the undeformed sediments below the colluvial wedge related to A3 and therefore occurred between 16.1 ± 1.7 ka and 48.9 ± 4.8 ka. The ages of A4 and A5 are similarly constrained in the trench SDF1 by sediments below and above the colluvial wegdes. Both events occurred between 56.6 ± 5.7 ka and 104 ± 12 ka.

In trench SDF3, samples (AIP93-AIP102) defining the chronology of the stratified hanging wall between 158 ± 21 ka and 4.8 ± 0.5 ka were dated in addition to two more samples (AIP103 and AIP114) determine the minimum age of the footwall to 205 ± 37 - 259 ± 35 ka. Those obtained ages agree well with other IRSL ages for the Gaenserndorf terrace (Weissl et al., 2017). In addition, IRSL data of the hanging wall constrain ~~roughly~~ the occurrence times of the 5 observed paleo-earthquakes along the main fault. While B1 is constrained to have occurred between 4.8 ± 0.5 ka and 32.9 ± 4.1 ka, B2 and B3 can only limited to occur together within the time interval between 32.9 ± 4.1 ka and 70.8 ± 8.0 ka. Also for B4 and B5, a common time interval between 111 ± 12 ka and 123 ± 16 ka can be determined. At the trench site WAG, both the uppermost and the lowermost sediments of the fine-graded silty to sandy cover were dated by IRSL revealing ages of 15.06 ± 1.52 ka and 16.1 ± 1.7 ka, respectively (samples AIP25, 26, Weissl et al., 2017).

Natural Hazards
and Earth System
Sciences
Discussions

## 5 Correlation of events between sites

Palaeoseismological investigations along the MF include three locations, the trenches SDF1 and SDF3 as well as the pipeline outcrop WAG. For all three locations, detailed mapping and dating have been carried out and described above. Evidence for 5 possible earthquakes have been observed in the trenches SDF1 (named A1-A5) and SDF3 (B1-B5), while in the pipeline

5    outcrop WAG, observations indicate two paleo-earthquakes (C1 and C2). Figure 10 shows the constraints of earthquake occurrence times for each observation point. Based on this information, together with comparison of trench observations and displacement estimates for all three outcrops, we correlate the observations and results to generate a synthesis of the earthquake occurrence along the MF. In the following, we discuss each earthquake and the possible correlations between the trenches as well as the resultant age, displacement and magnitude estimate, starting with the youngest.

10   **5.1 Event 1 (A1 = B1 = C1)**

In all three outcrops, the youngest event is evident from a measurable offset of layers across the MF. At trench site SDF1, the youngest event A1 shows displacements of 15-25 cm and occurred in the time range between $13.8 \pm 1.4$ ka and $16.3 \pm 1.8$ ka. At trench site SDF3, markers have been displaced by the youngest event B1 by 10-15 cm. The ISRL data limits the occurrence time of B1 to the time range between $4.8 \pm 0.5$ ka and $32.9 \pm 4.1$ ka. In the pipeline outcrop WAG, the loess cover is dated between $15.1 \pm 1.5$ ka and $16.1 \pm 1.7$ ka. It is displaced by 17-20 cm. Therefore, C1 must have happened after $15.1 \pm 1.5$ ka. The occurrence time for E1 is thus constraint to the time interval between $13.8 \pm 1.4$ ka and $15.1 \pm 1.5$ ka (Table 2). Using the empiric relationship between surface displacement and magnitude (Wells and Coppersmith, 1994) for the maximum displacement of 25 cm, E1 had the magnitude $M = 6.2 \pm 0.2$. The average displacement of 17 cm would lead to a similar magnitude $M = 6.3 \pm 0.3$.

20   **5.2 Event 2 (A2 = B2 = C2)**

Event E2 is also observed in all three outcrops as a triangular-shaped colluvial wedge mainly consisting of reworked gravels that derived from the terrace in the footwall. In addition, the top of each of those colluvial wedge deposits is displaced by E1, confirming the correlation of the colluvial wedges to the penultimate seismic event E2. At trench site SDF1, the displacement related to A2 (1.5-1.9 m) is estimated from the height of the associated colluvial wedge (0.75 - 0.95 m). IRSL samples constrain

25   the occurrence time for A2 to the time interval between $16.1 \pm 1.7$ ka and $48.9 \pm 4.8$ ka. At trench site SDF3, the interpretation of deposits related to B2 are more ambiguous (see sec. 3.2), and therefore, the estimated displacement is either 0.8 m (collapsed free face scenario) or 1.6 m (colluvial wedge scenario). B2 is constrained between $32.9 \pm 4.1$ ka and $70.8 \pm 8.0$ ka. In the pipeline construction pit the displacement of E2 can only be constrained to exceed 1 m by the colluvial wedge as the base of the wedge is not exposed. Time constraints are limited to the ante quem of $16.1 \pm 1.7$ ka by the age of the overlying loess

30   covering the colluvial wedge.

Combining the individual time constraints in each trench site allow to determine the occurrence time of E2 between $32.9 \pm 4.1$ ka and $48.9 \pm 4.8$ ka. Magnitude calculation using the maximum of the observed surface displacements results in a magnitude of M = $6.8 \pm 0.1$) (Wells and Coppersmith, 1994). With the maximum value for the observed surface displacement coming from trench SDF1, the magnitude estimate does not depend on the interpretation for the B2 deposits in trench SDF3.

**5.3 Event 3 (A3, probably correlated with B3)**

For this event, a correlation based on field observations between the trenches SDF1 and SDF3 is not as clear as in the cases of E1 and E2, especially since the evidence for B3 does not allow to determine a displacement for this possible event. However, the maximum height of a well-developed sandy colluvial wedge in SDF1 gives a good estimate of an earthquake with M = $6.6 \pm 0.1$. Because of the similar stratigraphic constraints, the possible occurrence time of E3 is constrained by the same limits as E2, so that E3 occurred also between $32.9 \pm 4.1$ ka and $48.9 \pm 4.8$ ka.

**5.4 Event 4 (A4, if correlated with B3)**

Another possible correlation scenario between the trench sites SDF1 and SFD3 is the correlation of A4 and B3 (event line 1 in Figure 10), mainly due the loose time constraint of B3. If A4 and B3 are correlated to the same seismic event E4, the overlap of possible occurrence times of A4 and B3 narrows the resultant occurrence time for E4 to the interval between $56.6 \pm 5.7$ ka and $70.8 \pm 8.0$ ka. Observations of the maximum wedge height at trench site SDF1 indicate the magnitude of A4 (and therefore for E4) to M = $6.8 \pm 0.2$.

**5.5 Event 5 (A4, if correlated with B4)**

In an alternative scenario, A4 could also correlate to B4 (event line 2 in Figure 10). In this case, the combined occurrence time for the resultant seismic event E5 must be older than $111 \pm 12$ ka and younger than $104 \pm 12$ ka. Thus, the time constraint would be thigh, dating E5 to the overlap of the uncertainties of the IRSL age dating between 100 ka and 116 ka with a mean at $107.9 \pm 8.0$ ka. Similar to E4, the magnitude for E5 can be estimated from the observations of the maximum wedge height of A4 at trench site SDF1, indicating a magnitude for E5 of M = $6.8 \pm 0.2$.

**5.6 Event 6 (possible correlation between A5 and B4) and Event 7 (possible correlation between A5 and B5)**

The later back in time, the more uncertain the correlation between both trench sites becomes. So, whether A5 and B5 are correlated to one event E6 or A5 and B4 are correlated to one event E7 is not clearly determined neither by observations nor dating. Both alternatives are possible and only depend on whether A4 is correlated to B3 or to B4. In event line 1, where A4 s correlated with B3, it appears reasonable to assume subsequently that A5 = B4. In contrast, if A4 = B4 (event line 2), the remaining correlation for the next older event would be A5 = B5. Due to the loose time constraints in the lower part of all trenches, the occurrence times for E6 and E7 are identical to those used for E5, leading to a time window of approximately

100-116 ka where either E6 or E7 occurred. Since both magnitude estimates for E6 and E7 are based on the maximum colluvial wedge height of A5 from SDF1, the magnitude of E6 and E7 is M = 6.5 ± 0.1)

### 5.7 Event 8 (B5, if not correlated with any event in SDF1)

In the case that B5 is not correlated with any events recorded in trench SDF1 (event line 1), the timing of E8 would be bracketed by the age dating s of 111 ± 12 ka and 123 ± 16 ka. E8 would therefore slightly older than E6 and E7. This would also imply that E8 might be older than the oldest deposits in SDF1 and therefore not visible there. Unfortunately, the magnitude of this possible seismic event cannot be constrained by trench observations.

### 6 Seismotectonic implications

### 6.1 Recurrence intervals for earthquakes with magnitudes larger than 6.5 along the MF

The possible correlations of paleoearthquakes between the trenches allow for two different interpretations to reconstruct the recurrence intervals of earthquakes with magnitudes larger than M = 6.5. The event E1 will be excluded during the following considerations, since the related magnitude estimate is lower than those obtained for E2-E7. It seems that the colluvial wedges associated with the larger earthquakes conceal or even erase evidences for offsets formed by smaller earthquake. The displacement of markers related to E1 is only conserved because the event happened after the last earthquake that caused a colluvial wedge to form (E2). Any future event with a surface displacement that is large enough to lead to the erosion of the offset markers in the footwall will destroy the evidence for E1. This restriction also applies to earthquakes with small surface offset that occurred prior to E2. Therefore, earthquake records for magnitudes less than about 6.5 are most probably incomplete, and thus excluded from the recurrence calculation.

As mentioned in sect. 5, the crucial part for the reconstruction of recurrence intervals therefore is whether A4 is correlated either to B3 or to B4 and, subsequently, whether A5 is correlated to B4 or to B5, resulting in the following event lines:

(1) E2-E3(not correlated to B3)-E4-E6-E8 (5 earthquakes);

(2) E2-E3(correlated to B3)-E5-E7 (4 earthquakes).

The determination of inter-event intervals is based on the limits for the occurrence time intervals for each earthquake as given in Table 2. Figure 10 shows clearly that both event lines represent different types of distributing earthquakes.

Event line 1 represents an approximately periodic reoccurrence of earthquakes with magnitudes larger than M = 6.5. The maximum time interval between E2 and E3 is 15.8 ka. As the occurrence time of E3 limits the occurrence time interval of E2, the minimum time interval cannot be calculated. Considering event line 1 (E2-E3-E4-E6-E8) and the range of uncertainties related to dating, the inter-event time between E3 and E4 lies between 6.3 ka and 41.5 ka, while the inter-event time between E4 and E6 is between 20.2 ka and 65.1 ka. Finally, the maximal inter-event time between E6 and E8 is constrained to 40 ka. Similar to the inter-event time for E2/E3, a minimum inter-event time for E6/ E8 cannot be calculated. Taking all information

together, the average of the minimum values and the average of the maximum recurrence intervals for event line 1 would be then ~ 13 ka and ~ 40 ka, respectively.

On the other side, earthquakes in event line 2 (E2-E3-E5-E7) seem to cluster in time. Therefore, instead of calculating inter-event times for all earthquakes, we calculate the minimum inter-cluster time that is identical with the inter-event time for E3/E5, and the maximum intra-cluster times for E2/E3 and E5/E7, meaning the largest possible time between both earthquakes within the same cluster. A maximal inter-cluster time cannot be given, due to the poor time constraint within the both clusters. However, the maximal intra-cluster times for E2/E3 and E5/E7 are 15.8 ka and 17.0 ka, respectively. In addition, the minimum inter-cluster time interval between E2/E3 and E5/E7 is at least 54.4 ka. The time since the occurrence of E2 until today may be also considered as a minimum inter-cluster time, being at least $32.9 \pm 4.1$ ka and maximal $40.9 \pm 3.6$ ka. Another estimation of the minimum elapse time between clusters can be estimated from the oldest layers in trench SDF3 (unit 8) dated to $158 \pm 21$ ka (sect. 3.2). Since there is no older record than B5, it is reasonable to assume that there was no earthquake during the time between B5 and the oldest unit 8 exposed in SDF3. Therefore, the minimum time elapsed between B5 (=E7) and any older cluster must be at least $42 \pm 21$ ka.

## 6.1 Comparison of long-term Quaternary slip rates with paleoseismological slip rates

Long-term Quaternary slip rates along the MF can be inferred from using the morphological scarp height of about 17 m and the age of the top of the Gaenserndorf terrace (~ 200 ka, Weissl et al., 2017). Using the present-day scarp height as minimum displacement since the abandonment of the terrace 200 ka ago, a minimum slip rate of 0.085 mm/a may be assumed. In addition, the base of the Quaternary gravels, which is equivalent to the top of Neogene sediments, is offset by approximately 40 m (Figure 3). Assuming that this should have happened after the Neogene-Quaternary boundary (2.6 Ma), the slip rate along the MF should be larger than 0.015 mm/a. It must be noted that this is a minimum estimate since age data from the thick Quaternary sediments in the hangingwall of the MF are not available. Figure 11 shows the range of possible slip rates for both event lines falling in between the bracket of the geomorphic slip rates, showing a reasonable agreement.

## 6.3 Comparison of magnitude estimates with fault rupture area and length

For faults with known fault geometry, empiric relations allow to evaluate the maximum magnitude that a fault can produce from rupture length and area. The surface expression of the MF is only recognizable for about 10 km along the eastern margin of the Pleistocene Gaenserdorf terrace (Figure 3A). Further to the south, the Danube has erased any geomorphic expression in its Holocene flood plain. However, the geometry and the length of the MF are well known thanks to the distribution of Quaternary sediments in the hangingwall of the fault and 2D/3D reflection seismic within the central Vienna Basin (Hölzel et al., 2010, Hinsch and Decker, 2011, Salcher et al., 2012, Spahic et al., 2013). Based on these data, the length of the MF as an isolated fault is around 25 km (Salcher et al., 2012). In addition, Hinsch and Decker (20 constructed a generalized detachment for the Vienna Basin. Beneath the MF, the detachment is assumed to be at the depth of about 10 km (Wessely et

al., 2006). Taking into account the general dip of 55° for the MF observed in seismic, the rupture area of the MF would amount to 315 km², leading to a maximal credible magnitude of 6.5 ± 0.3).

However, in case that the MF is indeed linked to the VBTF via the common detachment as proposed by Beidinger and Decker (2011), the area of the detachment between the MF and VBTF might be also activated during large events (Figure 12). The

5 total fault surface activated during such events is derived as the sum of the fault surface of the MF and the portion of the basal detachment between the MF and the VBTF, which has a size of about 130 km². The fault length of the MF in this tectonic scenario is 36 km and the total fault area amounts to about 580 km². These fault parameters correspond to a maximal credible magnitude of 6.7 ± 0.3) using the relationships by Wells and Coppersmith (1994). This is in good agreement to the magnitude estimations derived from the trenches.


10 **7 Conclusions and implications for seismic hazard assessment**

In this study, we provide evidence for the seismogenic character of a splay normal fault of the VBTF that previously has not been considered as a source for seismic hazards. We show evidence that the fault caused at least 5-6 strong earthquakes with magnitudes larger than 6.2 in the last 120 ka. The magnitude of the earthquake with the largest surface displacement is evaluated with 6.8 ± 0.1). This value compares well with the maximum magnitude of 6.7 ± 0.3) estimated from the potential

15 rupture area of the MF. The fault area is about 580 km² when including the detachment that links the normal fault with the VBTF. The vertical slip velocity of 0.03 to 0.04 mm/a derived from trench observations lies well within the geomorphologically determined vertical slip rates for the MF, which range from 0.085 to 0.015 mm/a.

Trench observations and uncertainties of OSL/IRSL age dating do not allow for an unequivocal conclusion of earthquake recurrence rates. Both earthquake scenarios (event lines 1 and 2) presented here are possible considering the available time

20 constraints. Event line 1, however, appears less likely as it seems improbable that an earthquake with a magnitude around 6.6 has not been recorded in trench SDF3, while producing a surface displacement of 80-90 cm in trench SDF1 at a distance of less than 2 km. For us, the more plausible correlation between the trenches is therefore event line 2, suggesting that earthquakes with magnitudes larger than 6.5 cluster in time. This may have consequences for the application of the reconstructed recurrence intervals in seismic hazard assessments, e.g., by using cluster recurrence intervals rather than average single event recurrence

25 intervals.

Trench evidence for the youngest event E1 (magnitude 6.2 ± 0.2) further shows that strong earthquakes with magnitudes less than 6.5 also occur outside of the suggested clusters. Unfortunately, the recurrence intervals of such events cannot be constrained by trenching results. The sedimentary and structural records of events with surface displacements, which are too small to produce colluvial wedges, may be masked or even erased by subsequent larger earthquakes that lead to the erosion

30 and redeposition of material into colluvial wedges. Therefore, earthquake records for magnitudes less than about 6.5 are most probably incomplete at the MF.

The issues discussed above lead us to conclude the following main implications for seismic hazard assessment in the Vienna Basin:

1.  The paleoseismological results ~~from the MF prove that it~~ is seismically active and ~~needs~~ to be considered as a seismogenic source in seismic hazard assessment. Earthquakes with magnitudes larger than about 6.5 occur at average recurrence times of about 25 ka (~~event line~~ 1), ~~or, more likely, in clusters~~ (~~event line~~ 2; Figures 10 and 11). The frequency of surface-breaking earthquakes with magnitudes less than about 6.5 cannot be constrained by trenching due to the low preservation potential of such earthquake records.

2.  Data from the MF provides evidence that the maximum credible earthquakes in the Vienna Basin ~~should~~ ~~not~~ ~~be considered to be about M=7.0.~~ This value is significantly higher than previous estimates of Mmax = 6.0 to 6.5 (Lenhardt et al., 1995; Procházková and Šimunek, 1998; Sefara et al., 1998; Tóth et al., 2006). The data presented in our study was used in the SHARE project to incorporate the MF in its active fault database and hazard calculation (Basili et al., 2013).

3.  The MF is kinematically and geologically ~~equivalent~~ to a number of other splay normal faults of the VBTF close to the Austrian capital, Vienna (Figure 9; Beidinger and Decker, 2011). It ~~must be assumed~~ that these faults are potential sources of large earthquakes as well. However, except for the Aderklaa-Bockfliess faults (Weissl et al., 2017), no paleoseismic characterisation of these faults ~~exists so far.~~ The frequency of strong earthquakes near Vienna is therefore expected to be ~~significantly~~ higher than the earthquake frequency reconstructed for the MF.

4.  The magnitude of the largest earthquake recorded at the MF (6.8 ± 0.1) is regarded to support the assumption of a listric fault and an active basal detachment that links the normal fault with the VBTF strike-slip system. ~~This~~ fault geometry ~~has severe consequences for the~~ ground motion ~~pattern related~~ to earthquakes that activate large parts of the listric fault with ground motion expected to be more severe in the hanging wall direction, than in the footwall direction (Passone and Mai, 2016). Although such directivity effects may reduce the hazard arising from the MF for Vienna, the opposite is true for other listric faults stretching into the city limits of Vienna (Figure 12).

Natural Hazards
and Earth System
Sciences
Discussions

# References

Basili R., Kastelic V., Demircioglu M. B., Garcia Moreno D., Nemser E. S., Petricca P., Sboras S. P., Besana-Ostman G. M., Beidinger, A. and Decker, K., 3D geometry and kinematics of the Lassee flower structure: Implications for segmentation and seismotectonics of the Vienna Basin strike–slip fault, Austria, Tectonophysics, 499, 22-40, doi:10.1016/j.tecto.2010.11.006,

5  2011.

Blair M.W., Yukihara, E.G., and McKeever, S.W.S., Experiences with single aliquot OSL procedures using coarse-grain feldspars, Radiat. Meas., 39, 361-374, 2005.

Bøtter-Jensen, L., Bulur, E., Duller, G.A.T., and Murray, A.S., Advances in luminescence instrument systems, Radiat. Meas., 32, 523–528, 2000.

10  Cabral J., Camelbeeck T., Caputo R., Danciu L., Domac H., Fonseca J., García-Mayordomo J., Giardini D., Glavatovic B., Gulen L., Ince Y., Pavlides S., Sesetyan K., Tarabusi G., Tiberti M. M., Utkucu M., Valensise G., Vanneste K., Vilanova S., Wössner J., The European Database of Seismogenic Faults (EDSF) compiled in the framework of the Project SHARE. http://diss.rm.ingv.it/share-edsf/, doi:10.6092/INGV.IT-SHARE-EDSF, 2013.

Camelbeeck, T., Alexandre, P., Vanneste, K. and Meghraoui, M., Long-term seismicity in regions of present day low seismic

15  activity: the example of Western Europe. Soil Dyn. Earthq. Eng., 20, 405-414, 2000.

Camelbeeck, T. and Meghraoui, M., Geological and geophysical evidence for large palaeo-earthquakes with surface faulting in the Roer Graben (northwest Europe). Geophys. J. Int., 132, 347-362, 1998.

Camelbeeck, T., Vanneste, K., Alexandre, P., Verbeeck, K., Petermans, T., Rosset, P., Everaerts, Warnant, R., and van Camp, M., Relevance of active faulting and seismicity studies to assessments of long-term earthquake activity and maximum

20  magnitude in intraplate northwest Europe, between the Lower Rhine Embayment and the North Sea. Geol. Soc. Am. Spec. Pap. 425, 193-224, 2007.

Chwatal, W, Decker, K., and Roch, K.-H., Mapping of active capable faults by high-resolution geophysical methods: examples from the central Vienna Basin. Austrian J. Earth Sci., 97, 52-59, 2005.

Clark, C., McPherson, M, van Dissen, R., Long-term behaviour of Australian stable continental region (SCR) faults.

25  Tectonophysics, 566-567, 1-30, 2012.

Decker, K., Gangl, G., and Kandler, M., The earthquake of Carnuntum in the 4th century AD - archaeologic results, seismologic scenario and seismo-tectonic implications for the Vienna Basin Fault, Austria. J. Seismol., 10, 479-495, 2006.

Decker, K., Gruppe, S. and Hintersberger, E., Characterizing active faults in the urban area of Vienna, Miscellanea INGV, 27, 212-215, 2015

30  Decker, K., Peresson, H., and Hinsch, R, Active tectonics and Quaternary basin formation along the Vienna Basin Transform fault. Quaternary Sci. Rev., 24, 305-320, 2005.

Natural Hazards
and Earth System
Sciences
Discussions

EGU

Open Access

Friedrich, A. M., Wernicke, B. P., Niemi, N. A., Bennett, R. A., and J. L. Davis, Comparison of geodetic and geologic data from the Wasatch region, Utah, and implications for the spectral character of Earth deformation at periods of 10 to 10 million years, J. Geophys. Res., 108, 2199, B4, doi:10.1029/2001JB000682, 2003.

Galbraith, R.F., Roberts, R.G., Laslett, G.M., Yoshida, H., and Olley, J.M., Optical dating of single and multiple grains of
5    quartz from Jinmium rock shelter, northern Australia: Part I, experimental design and statistical models. Archaeometry, 41, 339-364, 1999.

Gutdeutsch, R., Hammerl, C., Mayer, I., and Vocelka K., Erdbeben als historisches Ereignis – Die Rekonstruktion des niederösterreichischen Erdbebens von 1590. Springer Verlag Wien, Heidelberg, New York, 1987.

Grenerczy, G., Sella, G., Stein, S., and Kenyeres, A., Tectonic implications of the GPS velocity field in the northern Adriatic
10   region. Geophys. Res. Lett., 32, L16311, doi: 10.1029/2005GL022947, 2005.

Grünthal, G.., Wahlström, R. and Stromeyer, D., The unified catalogue of earthquakes in central, northern, and northwestern Europe (CENEC) - updated and expanded to the last millennium. J. Seismol., 13, 517-541, 2009.

Hinsch, R., Decker, K., and Wagreich, M., 3-D mapping of segmented active faults in the southern Vienna Basin. Quaternary Sci. Rev., 24, 321-336, 2005.

15   Hinsch, R. and Decker, K., Seismic slip rates, potential subsurface rupture areas and seismic potential of the Vienna Basin Transfer Fault, Int. J. Earth Sci. (Geol. Rundsch.), 100, 1925 -1935, doi:10.1007/s00531-010-0613-3, 2011.

Hölzel, M., Decker, K., Zámolyi, A., Strauss, P., and Wagreich, M., Lower Miocene structural evolution of the central Vienna Basin (Austria). Mar. Petrol. Geol., 27, 666-681, doi:10.1016/j.marpetgeo.2009.10.0052010.

Lenhardt, W. A., Regional earthquake hazard in Austria. In: 10th European Conference on Earthquake Engineering G. Duma,
20   (ed.), Balkema, Rotterdam, 63-68, 1995.

Lenhardt, W., Svancera, J., Melichar, P., Pazdirkova, J., Havir, J., and Sykorova, Z., Seismic activity of the Alpine-Carpathian-Bohemian Massif region with regard to geological and potential field data. Geol. Carpath., 58, 397-412, 2007.

Liu, M., Stein, S., and Wang, H., 2000 years of migrating earthquakes in North China: How earthquakes in midcontinents differ from those at plate boundaries, Lithosphere 3, 128-132, doi:10.1130/L129.1, 2011.

25   Linzer, H. G., Decker, K., Peresson, H., Dell'Mour, R., and Frisch, W., Balancing lateral orogenic float of the Eastern Alps. Tectonophysics, 354, 211-237, doi:10.1016/S0040-1951(02)00337-2, 2002.

Linzer, H. G., Moser, F., Nemes, F., Ratschbacher, L., and Sperner, B. Build-up and dismembering of the eastern Northern Calcareous Alps. Tectonophysics, 272, 97-124, doi:10.1016/S0040-1951(02)00337-2, 1997.

McCalpin, J., Paleoseismology, 2nd ed., International Geophysics Series, 95, 613 p., 2008.

30   Meghraoui, M., Delouis, B., Ferry, M., Giardini, D., Huggenberger, P., Spottke, I., and Granet, M., Active Normal Faulting in the Upper Rhine Graben and Paleoseismic Identification of the 1356 Basel Earthquake. Science, 293, 2070-2073, 2001.

Passone, L. and Mai, M., Effects of listricity on near field ground motions: the kinematic case, Geophysical Research Abstracts, 18, EGU2016-7231, 2016.

Peters, G., Buchmann, T., Connolly, P., van Balen, R.T., Wenzel, F., and Cloetingh, S., Interplay between tectonic, fluvial and erosional processes along the Western Border Fault of the northern Upper Rhine Graben, Germany. Tectonophysics, 406, 39-66, 2005.

Preusser, F., Degering, D., Fuchs, M., Hilgers, A., Kadereit, A., Klasen, N., Krbetschek, M., Richter, D., and Spencer, J.,
5   Luminescence dating: basics, methods and applications, Eiszeitalter Gegenwart Quat. Sci. J., 57, 95–149, 2008

Procházková, D. and Šimunek, P., Fundamental data for determining seismic hazard for localities in Central Europe. Gradus, Praha, Czech Republic, 1998.

Ratschbacher, L., Frisch, W., Linzer, H.-G., and O. Merle, Lateral extrusion in the eastern Alps, Part 2: Structural analysis, Tectonics, 10(2), 257–271, doi:10.1029/90TC02623, 1991.

10   Rhodes, E., Optically stimulated luminescence dating of sediments over the past 200,000 years, Annu. Rev. Earth Planet. Sci., 39, 461–488, 2011.

Royden, L.H., The Vienna Basin: A thin skinned pull apart basin. In: Strike-slip deformation, basin formation, and sedimentation (Biddle, K.T. and Christie-Blick, N., Eds.). Tulsa, Oklahoma, USA, SEMP Special publications, 37, 319-340, 1985.

15   Salcher, B. C., Meurers, B., Smit, J., Decker, K., Hölzel, M., and Wagreich, M., Strike-slip tectonics and Quaternary basin formation along the Vienna Basin fault system inferred from Bouguer gravity derivatives. Tectonics, 31, doi: 10.1029/2011TC002979, 2012.

Šefara, J., Kováč, M., Plašienka, D., and Šujan, M., Seismogenic zones in the Eastern Alpine-Western Carpathian-Pannonian junction area. Geol. Carpath., 49, 247-260, 1998.

20   Spahic, D., Grasemann, B., and Exner, U., Identifying fault segments from 3D fault grad analysis (Vienna Basin, Austria). J. Struc. Geol., 55, 182-195, 2013.

Štěpančíková, P., Hók, P., Nývlt, D., Dohnal, J., Sýkorová, I., and Stemberk, J., Active tectonic research using trenching technique on the south-eastern section of the Sudetic Marginal Fault (NE Bohemian Massif, central Europe). Tectonophysics, 485, 269-282, 2010.

25   Tóth, L., Györi, E., Mónus, P., and Zsiros, T., Seismic hazard in the Pannonian region. In: The Adria Microplate: GPS Geodesy, Tectonics and Hazards (Pinter, N., Grenerczy, G., Weber, J., Stein, S. and Medak, D., Eds.) Springer Verlag, Dordrecht, the Netherlands, 369-384, 2006.

van den Berg, M., Vanneste, K., Dost, B., Lokhorst, A, van Eijk, M, and Verbeeck, K., Paleoseismic investigations along the Peel Boundary Fault: geological setting, site selection and trenching results. Neth. J. Geosci., 81, 39-60, 2002.

30   Vanneste, K., Camelbeeck, T., and Verbeeck, K., A model of composite seismic sources for the Lower Rhine Graben, Northwest Europe. Bull. Seismol. Soc. Am., 103, 984-1007, 2013.

Vanneste, K. and Verbeeck, K., Paleoseismological analysis of the Rurrand fault near Jülich, Roer Valley graben, Germany: Coseismic or aseismic faulting history? Neth. J. Geosci., 80, 155-169, 2001.

Wallace, R. E., Grouping and migration of surface faulting and variation in slip rates on faults in the Great Basin province, Bull. Seismol. Soc. Am., 77, 868–877, 1987,

Wallinga, J., Murray, A.S., Wintle, A.G., The single-aliquot regenerative-dose (SAR) protocol applied to coarse-grain feldspar. Radiat. Meas., 32, 529-533, 2000.

5    Weissl, M., Hintersberger, E., Lomax, J., Lüthgens, C., and Decker, K., Active tectonics and geomorphology of the Gaenserndorf Terrace in the Central Vienna Basin (Austria). Quatern. Int., in print, doi: 10.1016/j.quaint.2016.11.022, 2017.

Wessely, G., Wiener Becken, In: Wessely, G. (Ed.), Geologie der österreichischen Bundesländer: Niederösterreich, Geologische Bundesanstalt, Vienna, 189–226, 2006.

Wells, D.L. and Coppersmith, K.J., New Empirical Relationships among Magnitude, Rupture Length, Rupture Width, Rupture
10   Area, and Surface Displacement. Bull. Seismol. Soc. Am., 84, 974-1002, 1994.

Wintle, A.G., Luminescence dating: where it has been and where it is going, Boreas, 37, 471–482, 2008.

**Tables**

| Event # | Evidence | Thickness of colluvial wedge @ NE wall | Thickness of colluvial wedge @ SW wall | Displacement |
|---|---|---|---|---|
| A1 | displ | - | - | 0.15 - 0.25 m |
| A2 | cw, tc | 0.95 m | 0.75 m | 1.50 - 1.90 m |
| A3 | cw, tc | 0.45 m | 0.40 m | 0.80 - 0.90 m |
| A4 | cw, tc | 0.75 m | 0.72 m | 1.40 - 1.50 m |
| A5 | cw | 0.25 m | 0.40 m | 0.50 - 0.80 m |
| B1 | displ | - | - | 0.10 - 0.15 m |
| B2 | cw | | 0.8 | 0.8/1.6 m |
| B3 | tc | - | - | - |
| B4 | cw | - | - | - |
| B5 | cw | - | - | - |
| C1 | displ | - | - | 0.17 - 0.20 m |
| C2 | cw | - | - | - |

**Table 1: Type of evidence and inferred displacement for the paleoearthquakes A1 to A5 (trench SDF1), B1 to B5 (SDF3), and C1 to C2 (WAG). Also listed are the thicknesses of colluvial wedges observed in the NW and SE trench walls used for estimating displacement. Evidence: displacement of correlated layers (displ.), occurrence of colluvial wedges (cw), and sediment-filled tension**
5 **cracks below the colluvial wedges (tc). Displacement is taken as twice the thickness of the colluvial wedge.**

| Sample | Location | Method | De (Gy) | $D_0$ (Gy/ka) | Depth (m) | Water (%) | Age (ka) |
|---|---|---|---|---|---|---|---|
| AIP25 | WAG cover | IRSL | $44.7 \pm 2.3$ | $2.78 \pm 0.26$ | 1.0 | 12 | $16.1 \pm 1.7$ |
| AIP26 | WAG cover | IRSL | $39.0 \pm 1.4$ | $2.01 \pm 0.16$ | 0.5 | 12 | $15.1 \pm 1.5$ |
| AIP38 | SDF1 fw | IRSL | $543.1 \pm 33.7$ | $2.13 \pm 0.20$ | 3.7 | 10 | $255 \pm 29$ |
| AIP39 | SDF1 hw | IRSL | $273.5 \pm 20.2$ | $2.64 \pm 0.25$ | 3.6 | 10 | $104 \pm 12$ |
| AIP40 | SDF1 hw | IRSL | $154.0 \pm 5.5$ | $2.72 \pm 0.25$ | 3.3 | 10 | $56.6 \pm 5.7$ |
| AIP41 | SDF1 hw | IRSL | $168.7 \pm 5.9$ | $3.45 \pm 0.32$ | 2.6 | 10 | $48.9 \pm 4.8$ |
| AIP44 | SDF1 hw | IRSL | $36.7 \pm 2.1$ | $2.26 \pm 0.22$ | 1.9 | 10 | $16.3 \pm 1.8$ |
| AIP46 | SDF1 hw | IRSL | $43.6 \pm 1.6$ | $2.01 \pm 0.16$ | 1.2 | 10 | $13.8 \pm 1.4$ |
| AIP93 | SDF3 hw | IRSL | $419.2 \pm 39.4$ | $3.17 \pm 0.30$ | 4.1 | 12 | $158 \pm 21$ |
| AIP95 | SDF3 hw | IRSL | $317.4 \pm 29.1$ | $2.58 \pm 0.24$ | 3.1 | 12 | $123 \pm 16$ |
| AIP97 | SDF3 hw | IRSL | $205.1 \pm 13.3$ | $2.90 \pm 0.26$ | 2.1 | 12 | $70.8 \pm 8.0$ |
| AIP98 | SDF3 hw | IRSL | $91.6 \pm 7.5$ | $2.78 \pm 0.25$ | 1.8 | 12 | $32.9 \pm 4.1$ |
| AIP102 | SDF3 hw | IRSL | $15.7 \pm 0.9$ | $3.29 \pm 0.30$ | 0.3 | 15 | $4.8 \pm 0.5$ |
| AIP103 | SDF3 fw | IRSL | $384.6 \pm 59.7$ | $1.88 \pm 0.18$ | 1.4 | 10 | $205 \pm 37$ |
| AIP114 | SDF3 fw | IRSL | $468.3 \pm 43.4$ | $1.81 \pm 0.17$ | 0.65 | 10 | $259 \pm 35$ |

**Table 2: Infrared stimulated Luminescence (IRSL) and optically stimulated luminescence (OSL) dating results from the trenches SDF1, SDF3, and WAG at the Markgrafneusiedl Fault (MF). Location: refers to either of the trenches (SDF1, SDF3, WAG) and the**
10 **location in respect to the MF, where hw = hanging wall and fw = footwall, De (Gy): equivalent dose in Gray (Gy), $D_0$ (Gy/ka): dose rate in Gray values (per 1.000 years); Depth (m): depth of the sampling location in meters below present-day surface.**

| Event # | Correlation | *Antequem* Event older than (age / sample location) | *Postquem* Event younger than (age / sample location) |
|---|---|---|---|
| E1 | A1 = B1 = C1 | **13.8 ± 1.4 ka (SDF1),** 4.8 ± 0.5 ka (SDF3) | 32.9 ± 4.1 ka (SDF3), 16.3 ± 1.8 ka (SDF1), **15.1 ± 1.5 ka (WAG)** |
| E2 | A2 = B2 = C2 | **32.9 ± 4.1 ka (SDF3),** 16.1 ± 1.7 ka (SDF1) | 70.8 ± 8.0 ka (SDF3), **48.9 ± 4.8 ka (SDF1)** |
| E3 | A3, ?= B3? | **32.9 ± 4.1 ka (SDF3),** 16.1 ± 1.7 ka (SDF1) | 70.8 ± 8.0 ka (SDF3), **48.9 ± 4.8 ka (SDF1)** |
| E4 | A4, ?= B3? | **56.6 ± 5.7 ka (SDF1)** 32.9 ± 4.1 ka (SDF3), | 104 ± 12 ka (SDF1), **70.8 ± 8.0 ka (SDF3)** |
| E5 | ?A4 =? B4 | **111 ± 12 ka (SDF3),** 56.6 ± 5.7 ka (SDF1) | 123 ± 16 ka (SDF3), **104 ± 12 ka (SDF1)** |
| E6 | A5 ?= B4? | **111 ± 12 ka (SDF3),** 56.6 ± 5.7 ka (SDF1) | 123 ± 16 ka (SDF3), **104 ± 12 ka (SDF1)** |
| E7 | ?A5 = B5? | **111 ± 12 ka (SDF3),** 56.6 ± 5.7 ka (SDF1) | 123 ± 16 ka (SDF3), **104 ± 12 ka (SDF1)** |
| E8 | B5 | **111 ± 12 ka (SDF3)** | **123 ± 16 ka (SDF3)** |

**Table 3: Overview of common IRSL constraint for each possible earthquake derived from all different sites. Ages in bold mark the upper and lower limit for each occurrence time. For details about correlation between the trenches, see sect. 5.**

**Figure captions**

Figure 1: A) ==Active== faults (black solid and dashed lines), seismicity (black circles) and Quaternary basins (light grey areas) within the Vienna Basin (Austria) plotted on a shaded DEM. The borders of the Austrian capital, Vienna, is outlined by a dashed white line. Modified after Beidinger and Decker (2011).  White box shows the location of the ~~close up~~ in Figure 2; (B) Major earthquakes

5  from historical, instrumental and paleoseismological data in intra-plate central Europe. Historical and instrumental seismicity is based on the CENEC Catalogue by Grünthal et al., 2009. ==Paleosites== are compiled from Camelbeeck and Meghraoui, 1998; Camelbeeck et al., 2000; 2007; Meghraoui et al., 2001; Vanneste and Verbeeck, 2001; van den Berg et al., 2002, Peters, et al., 2005; Štěpančíková et al., 2010. Labels indicate the magnitudes of the largest paleoearthquakes observed at the respective site. Black box shows area of the close up in (A). MF= Markgrafneusiedl Fault; VBTF = Vienna Basin ==Fault System.==

10  Figure 2: Cross section through the Vienna Basin at its central part based on reflection seismic and deep boreholes indicating the common detachment of the Alpine floor thrust, which links the splay normal faults to the Vienna Basin Transfer Fault (VBTF). Redrawn from Hölzel et al. (2010).

Figure 3: Overview of the MF. (A) DEM the Pleistocene terraces north of the Danube dissected by faults ~~creating fault scarps~~ (fs). Dashed line: trace of the topographic profile in B, solid line: trace of the seismic line in C. (B) Topographic profile (black) and cross-

15  section indicating the base of Quaternary sediments (grey) across the MF. ==Note the thickness of Quaternary growth strata in the fault-delimited basin above the MF.== (C) seismic section across the same area showing offset along the Markgrafneusiedl Fault (MF) and the flower structure at the Vienna Basin Transfer Fault (right). See text for details.

Figure 4: Photo mosaic and interpretation of the SW-facing wall of the trench SDF1 across the Markgrafneusiedl Fault (for location

20  see Figure 2). Colluvial wedges and underlying tension cracks related to earthquakes A2-A5 are numbered. The displacement related to A1 is marked. Numbers indicate the age and the location of IRSL and OSL samples.  See text for further explanation.

Figure 5: Details from the SW-facing wall of the trench SDF1. (A) Evidence for earthquake A1 from the displacement of a marker horizon (white arrows), which is correlated across the fault (red arrows). (b) Evidence for earthquake A2 from a colluvial wedge composed of sandy gravel overlying a tension gash filled with the same material (white arrows). To the right the wedge abuts against

25  fault 1 (red arrows). (C) Colluvial wedge associated with earthquake A3 (white arrows) overlying a tension gash adjacent to fault 2. Several deformation bands that branch from fault 2 and formed during a later earthquake cut the wedge. It overlies wedge 4, which equally contains reddish redeposited soil. Wedge 4 shows an erosional contact to grey high-stage flood sediments (around box E). (D) Deformation bands offsetting laminated fluvial sand (red arrows) above wedge 2. The deformation bands are correlated to the event horizon of E1 (detail of picture B). (E) Detail of (C). Erosional contact of wedge 4 to flood sediments. Armoured mudballs

30  (arrow) derive from the eroded colluvium.

Figure 6: Photo mosaic and interpretation of the SW-facing wall of the trench SDF3 across the Markgrafneusiedl Fault (for location see Figure 2). Colluvial wedges and underlying tension cracks related to earthquakes B2-B5 are numbered. The displacement related to B1 is marked. Numbers indicate the age and the location of IRSL and OSL samples. Additional information is provided in the

35  text.

**Figure 7:** Details from the SW-facing wall of the trench SDF3. **(A)** Wedge associated with earthquake B2 (white arrows; see text for discussion) overlying wide fault (red arrows). The upward widening fault is recognized from pebbles, which are oriented parallel to the fault. The top of the wedge (white arrows) is offset by a narrow deformation band that emerges from the fault below the wedge (purple arrows). Offset occurred during B1. **(B, C)** Laminated flood sediments (clay, silt and fine sand) underlying colluvium of

5    wedge B2. Pebbles sunken into the soft sediment (B) and flame structures protruding into the overlying gravel (C) are indicative for liquefaction.

**Figure 8: (A)** Trench WAG, photo mosaic of the SW-facing trench wall. Red arrows denote locations of faults, white arrows point to offset contact between colluvium and overlying loess. Boxes refer to details shown in Figure 9 B and C.

10

**Figure 9: (A)** Trench WAG looking E toward the footwall of the MF (fault trace denoted by red arrows). Note offset of bright layer of loess (white arrows) corresponding to C1. CW denotes the colluvial wedge related to earthquake C2. **(b)** Detail of the SW-facing trench wall. Red arrows denote locations of faults, white arrows point to the offset contact between grey and brown silt and clay. Box shows location of details shown in D. **(C)** Offset of the top of the colluvial wedge associated with earthquake C2 (white arrows).

15   **(D, E)** Fractured and sheared pebbles indicating normal displacement parallel to the slip of the MF. <mark>Note that fractures in pebbles are filled with sandy matrix excluding fracture formation during construction work.</mark>

**Figure 10:** Comparison of age constraints from all trench sites SDF1, SDF3, and WAG and possible occurrence times of the observed earthquakes for the two possible correlations.

20   **Figure 11:** Comparison of surface slip rates for the Markgrafneusiedl Fault (MF) from geomorphic constraints and from trench results. On the left the constraints for event line 1 are plotted, on the right, those for event line 2 are shown.

**Figure 12:** Geometry and fault area of the Markgrafneusiedl Fault (MF). Also shown are the Vienna Basin Transfer Fault (VBTF) and other active normal splay faults branching from the VBTF. ABF: Adreklaa-Bockfliess fault system; BNF: Bisamberg-Nussdorf fault; LF: Leopoldsdorf fault; SF: Seyring fault (redrawn from Decker et al., 2015). Broken grey line marks the city limits of Vienna.
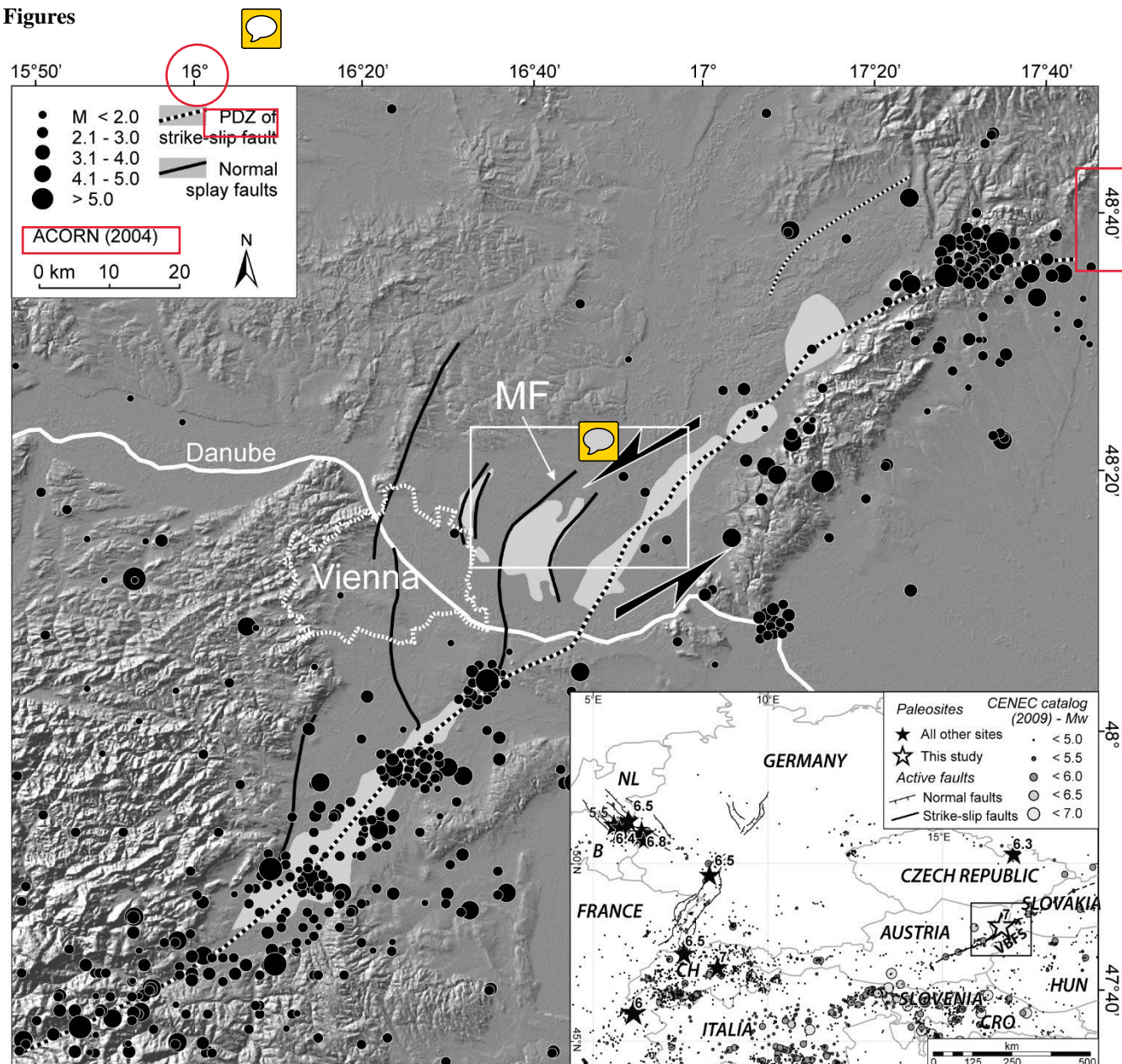
Natural Hazards
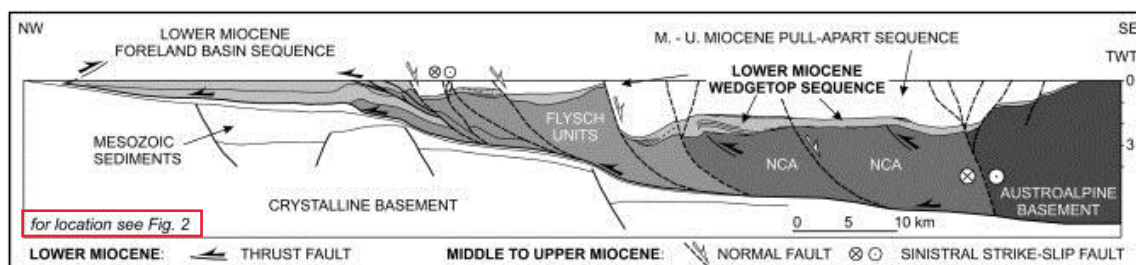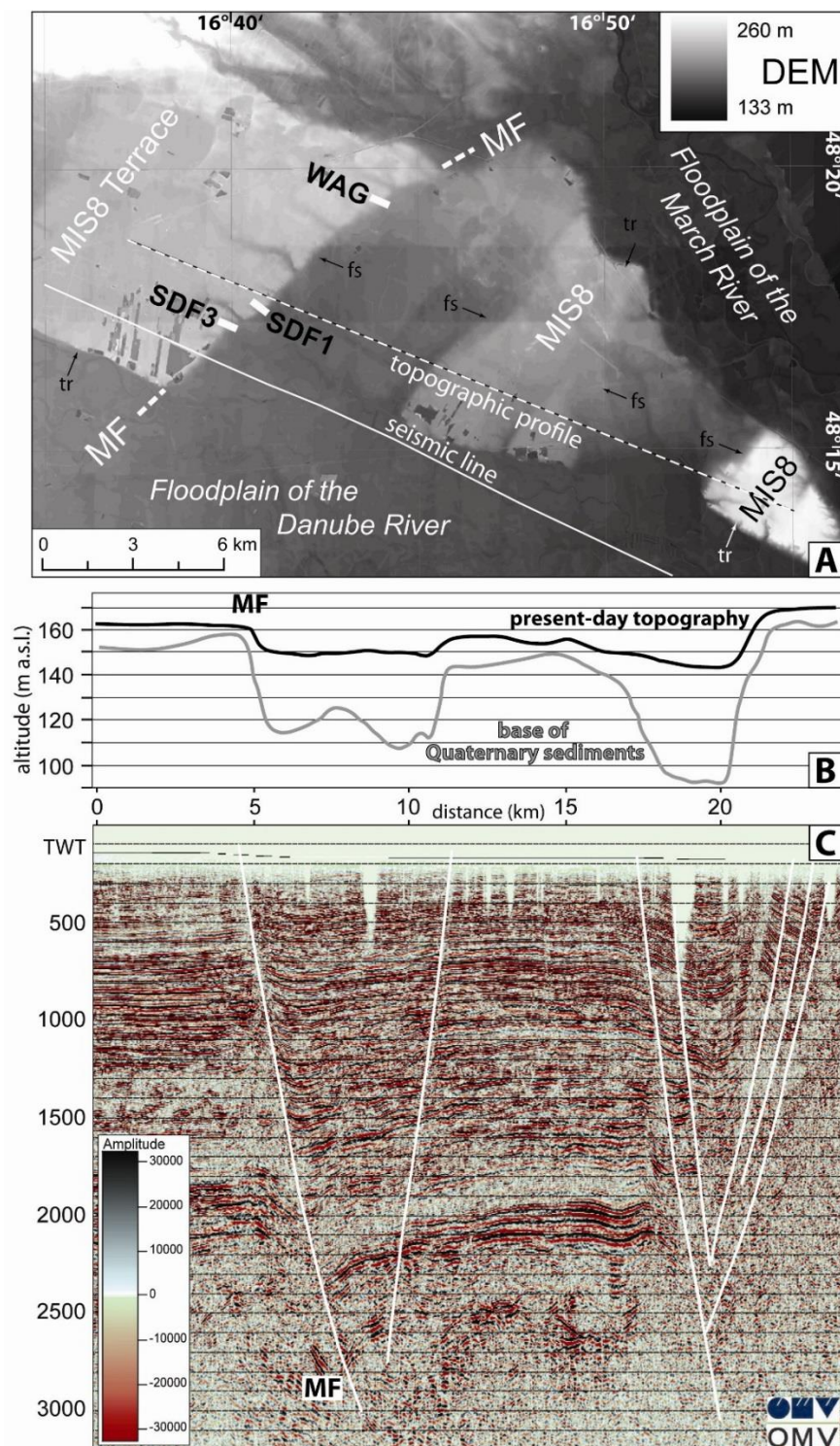and Earth System
Sciences
Discussions

**Figures**



**Figure 1**

**Figure 2**

**Figure 3**

Figure 4

Natural Hazards
and Earth System
Sciences

Discussions



**Figure 5**

Natural Hazards
and Earth System
Sciences
Discussions

Open Access



Figure 6

Natural Hazards
and Earth System
Sciences
Open Access
Discussions



Figure 7

Natural Hazards
and Earth System
Sciences

Open Access

Discussions

EGU



**Figure 8**

Natural Hazards
and Earth System
Sciences
Open Access
Discussions



**Figure 9**

5

**Figure 10**

Natural Hazards
and Earth System
Sciences

Open Access

Discussions



**Figure 11**

5



**Figure 12**